Multiturn ray-tracing based design study of a compact time of flight mass spectrometer ring

F. Méot[*], D. Michaud[†], M. Baril[†]

Proc. ICAP2000 Conf., Darmstadt, Germany, 11-14 Sept. 2000

December 26, 2005

Abstract

A design study of a low energy electrostatic storage ring employed as a multiturn time of flight mass spectrometer is presented. The design method is based on multiturn ray-tracing analysis and provides accurate tracking across highly non-linear electrostatic parallel-plate mirrors used as both focusing and bending optical elements in the spectrometer ring.

1 Introduction

The principle is admitted that multiturn storage is a convenient way to reach high resolution mass separation allied with small size apparatus [1]. Detailed studies on the electrostatic mirror [2, 3] have lead to considering it as a good candidate as both deflector and focusing optical element in an electrostatic low energy storage ring. Such a ring has recently been designed and is now under construction and experimental tests at Laval University [4, 5].

The present design work is based on high accuracy, large acceptance multiturn ray-tracing techniques [6], when regular matrix and other higher order mapping codes available prove to be unable to treat the problem in the present state of the art. The numerical method is based on the use of analytical models of electric fields and on stepwise ray-tracing from Taylor series expansion of particle coordinates (see Apps. A, B) ; this has the merit in particular of overcoming fringe fields and other field gradient issues. From ray-tracing simulation data, usual circular machine parameters are derived, along with time separation properties, a key feature in the utilization of the ring as a time of flight mass spectrometer (TOFMS).

2 Basis parameters, ring geometry

Fig. 1 shows the geometry of the periodicity-2 ring of concern, built from the symmetric cell (LV, LH, MA, MB, LH, LV) following first design using SIMION [7], wherein MA and MB are identical 3-electrode parallel-plate mirrors (App. B) acting as 90 degrees deflectors. Electrode potentials in

[*]CEA, DSM/DAPNIA/SEA, 91191 Saclay, France (fmeot@cea.fr)

[†]Université Laval, Départment de Physique, Sainte-Foy, Québec
(dmichaud@phy.ulaval.ca, baril@phy.ulaval.ca)

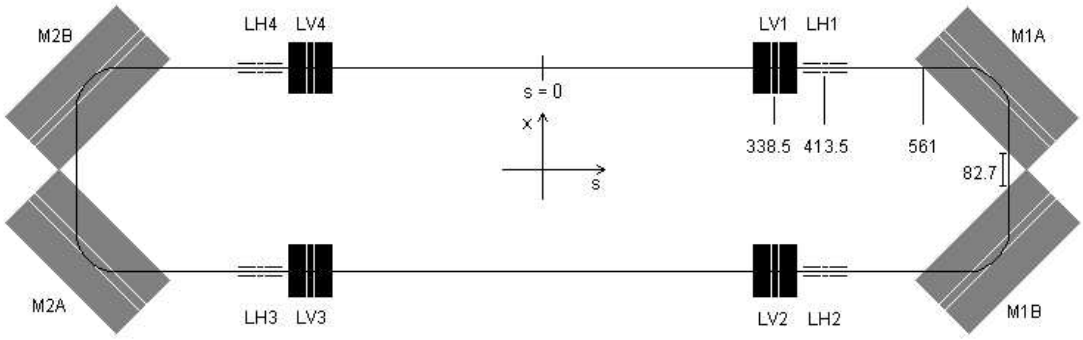

Figure 1: The TOFMS ring. Quotations are in millimeters.

MA, MB have been set to $V1 = 0, V2 = 173.2, V3 = 245.7$ Volts after earlier parameterization [8] ; the two 0.614 m long straight sections leave room for injection of the beam on one side and extraction on the opposite side of the ring [9] ; the 0.0827 m drift between MA and MB is kept short for compactness. LH and LV are 3-electrode parallel-plate unipotential transmission lenses and insure independent horizontal and vertical focusing ; potential $V2$ on their central electrode (noted respectively V_{LH}, V_{LV} in the sequel) is of a few tens of Volts allowing easy and accurate control of horizontal and vertical focusing, with typical stability limits $35 \lesssim V_{LH}, V_{LV} \lesssim 110$ Volts. The reference closed orbit is 3.2 m long, hence assuring high TOF resolution within a few turns (when conventionnal TOFMS beam lines do not exceed a few meters). Particles to be considered are somewhat arbitrary ; potential values above have been obtained with $T = 400$ eV single-charge N_2 with mass $M = 28$ uma $= 26.082\ 10^9$ eV ; the corresponding single turn duration for the central particle is 63.171 μs.

Coordinate system In the sequel a Serret-Frenet frame is used with $(x, x' = dx/ds)$ (respectively $(z, z' = dz/ds)$) describing the transverse horizontal (respectively vertical) motion, and s being the longitudinal coordinate around the closed reference orbit. Trajectory lengthening and energy deviation are noted respectively δl, $\delta E/E$.

3 General optical properties

Most features of the ring as presented below are specific to our concern and obtained from simple considerations and from numerical simulations based on ray-tracing. However they derive from the general optical properties of the electrostatic parallel-plate mirror that has already been subject to thorough analytical studies that one can refer to for more details [2, 3].

Optical aberrations

Optical aberrations of the (LV, LH, MA, MB, LH, LV) lattice cell (Figs. 1, 3) can be assessed from its second order transfer coefficients T_{ijk} $(i,j,k = 1-6)$ as defined by [10, p.85]

$$y_i(s) = \sum_{j=1}^{6} R_{ij} y_j(0) + \sum_{j=1}^{6}\sum_{k=1}^{6} T_{ijk} y_j(0) y_k(0) \tag{1}$$

wherein y_i stands for $x, x', z, z', \delta l$ or $\delta E/E$, R_{ij} and T_{ijk} are the Taylor expansion coefficients. General remarks can be drawn as to the present geometry (see Ref. [5] for more details) :

– horizontal aberrations : chromatic coefficients ($T_{1jk}, T_{2jk},\ j = 6$ or $k = 6$) are negligible ; coupling geometric terms ($T_{ijk},\ j \neq k$) are negligible, by contrast to the very strong parabolic terms ($T_{ijj},\ i = 1-2,\ j \neq 6$) that all are of order $10^4 - 10^6$;

– vertical aberrations : the only significant geometric terms are of coupling nature ($T_{ijk},\ i = 3-4,\ j,k = 1-2$) of order 1-10 ; there is some energy into vertical motion coupling ($T_{3jk}, T_{4jk},\ j$ or $k = 6,\ j \neq k$ of order 10-100) likely to induce energy acceptance limitation through vertical loss ;

– time resolution as related to particle mass has to cope with a large valued trajectory lengthening coefficient $\delta l\ /\ \delta E/E = R_{56} \approx 1$ responsible for harmful bunch lengthening (see Section 6). Optical corrections likely to minimize R_{56} are under study.

In a general manner, desirable minimization of second order geometrical transport coefficients suggests investigating the use of cylindrical mirrors for the MA, MB deflectors, according to Ref. [3], in view mostly of improving the vertical acceptance and the time resolution.

Transverse periodic stability

High time-resolution will require hundred turns flight, hence one main concern is long-term confinement of the beam along the TOFMS ring optical axis. This can be addressed in the following way.

Horizontal (respectively vertical) first order transverse stability is assessed from the horizontal one-turn transfer matrix $[R_{ij}]_{i,j=1,2}$ (respectively, $[R_{ij}]_{i,j=3,4}$) by identification with the Twiss form $I\cos(2\pi\nu) + J\sin(2\pi\nu)$ [10, p.103] wherein I is the identity matrix and J= $\begin{pmatrix} \alpha(s) & \beta(s) \\ -\gamma(s) & -\alpha(s) \end{pmatrix}$ with

$$\beta(s),\ 2\alpha(s) = -d\beta/ds,\ \gamma(s) = (1+\alpha(s)^2)/\beta(s) \tag{2}$$

being the optical functions at the observation azimuth s. Existence of the Twiss matrix is equivalent to stable periodic motion and imposes $(R_{ii} + R_{jj})/2 < 1$. In this case, paraxial particle trajectories in transverse phase space are ellipses with equation

$$\gamma(s)y^2 + 2\alpha(s)yy' + \beta(s)y'^2 = \epsilon/\pi \tag{3}$$

(y stands for either x or z), and with phase advance per turn

$$2\pi\nu = \int_{1turn} ds/\beta(s) \tag{4}$$

Single-cell matrices obtained from ray-tracing data show that stable periodic motion in both planes can only be obtained if $35 \lesssim V_{LH,LV} \lesssim 110$ Volts, which determines over that range a convenient tuning margin $\Delta\nu_{x,z} \approx 1$ with ratios

$$\Delta\nu_x/\Delta V_{LH} \approx \Delta\nu_z/\Delta V_{LV} \approx 0.012 \text{ per Volt} \tag{5}$$

and negligible cross ratios $\Delta\nu_x/\Delta V_{LV}$ and $\Delta\nu_z/\Delta V_{LH}$ as expected.

Tunes The fractional part of the tunes ν_x, ν_z can be obtained from Fourier analysis of multiturn ray-tracing, this is the method used in the sequel, that offers very good accuracy. The integer part of tunes in presence of electrostatic fields can be obtained from the one-turn phase advance (Eq. 4) ; this has been performed from matrix transport[1] using the dedicated J-language software described in Ref. [4] ; this for instance delivers in the present conditions, $\nu_z = 2$+fractional part. The knowledge of the total tunes further allows placing the working point in the tune diagram and checking such features as its straddling possible harmful resonances.

Chromaticity Tune calculations at intermediates potential values $V_{LH} \approx V_{LV} \approx 75$ Volts yield weak horizontal energy detuning $\Delta\nu_x \,/\, \delta E/E \approx 0.02$, and rather sensible vertical one $\Delta\nu_z \,/\, \delta E/E \approx -1$ that prognosticates tune spread induced energy limited acceptance, as corroborated by the 6-D tracking simulations of Section 5. Although this feature is not too detrimental in the present use as a TOFMS where only a few tens of turns are aimed at, methods for obtaining second or higher order vertical and to a less extent horizontal chromaticity compensation would need investigating if second or longer duration storage were to be achieved.

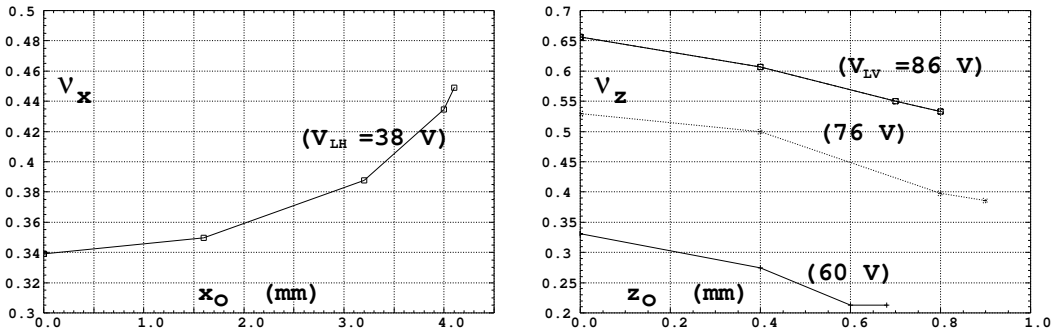

Figure 2: Horizontal and vertical fractional tunes (obtained from multiturn Fourier analysis) as a function of the particle starting transverse position (with zero angle) at $s = 0$.

amplitude detuning The optics features rather large detuning with increasing amplitude of the transverse motion (Fig. 2), again liable to alter transverse acceptance. This is addressed in Section 4.

[1] By transporting around the ring the two particular solutions of the Hill equation, $(y_1, y_1')_{s=0} = (\sqrt{\beta}, -\alpha\sqrt{\beta})_{s=0}$, $(y_2, y_2')_{s=0} = (0, -1/\sqrt{\beta})_{s=0}$ thus providing $\beta(s) = y_1^2(s) + y_2^2(s)$

Periodic dispersion

A basic property of the MA, MB symmetric mirror pair arrangement is in its being achromatic to all orders, for geometrical reasons : merged trajectories with distinct energies find themselves separate and parallel at exit of the first mirror MA (Fig. 3) and by symmetry are merged again at the exit of the second mirror MB. As a consequence the periodic horizontal dispersion function

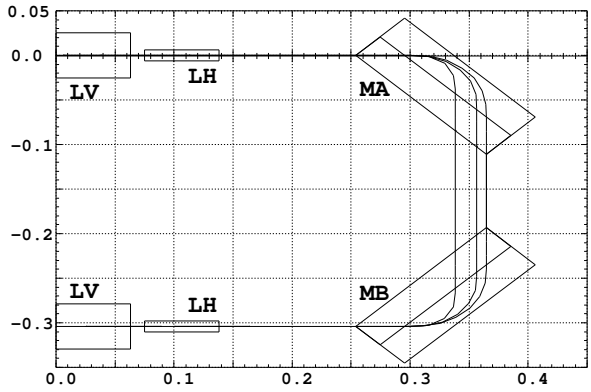

Figure 3: Trajectories over the half-ring (1 cell), of three ions having $\delta E/E = -20\%,\ 0$ and $+10\%$ energy dispersion. This is also a representation of the dispersion function $D_x(s) = \delta x(s)/\delta E/E$ that takes the constant value 0.1975 m in the short straight section between MA and MB and is identically zero in the long straight section.

$D_x(s) = \delta x(s)/\delta E/E$ (with periodicity that of the cell) is zero in the long straight sections, which eases beam injection and extraction, and takes its maximum value along the short MA-MB drifts. The vertical dispersion function $D_z(s)$ is identically zero due to the mid-plane symmetry of the optical elements.

Beam envelopes

Linear beam envelopes along the ring are defined by

$$\sigma_x(s) = \sqrt{\beta_x(s)\epsilon_x/\pi}, \quad \sigma_z(s) = \sqrt{\beta_z(s)\epsilon_z/\pi}, \tag{6}$$

with $\beta_{x,z}(s)$ and $\epsilon_{x,z}$ as given by Eqs. 3 ; their analytical calculation in presence of damping due to the varying energy (inside electrostatic optical elements) is described in Ref. [4]. They are in the present report derived from ray-tracing data : the paraxial horizontal envelope shown in Fig. 4 turns out to be very smooth, whereas the vertical one (Fig. 5) shows on the one hand very low β_z regions within the MA and MB deflectors that contribute strongly to the tune value ν_z, and on the other correspondingly large balancing β_z values that will cause sensitivity to field and positioning defects (that point still needs be worked out).

However as to the vertical motion, the linear approximation above fails at small distance off optical axis due to the strongly non-linear behavior of the electric field in the parallel-plate mirror (App. B). This is clearly observable in the $\nu_z \approx$half-integer case through a periodicity of 2 turns restoring orbit (Fig. 5).

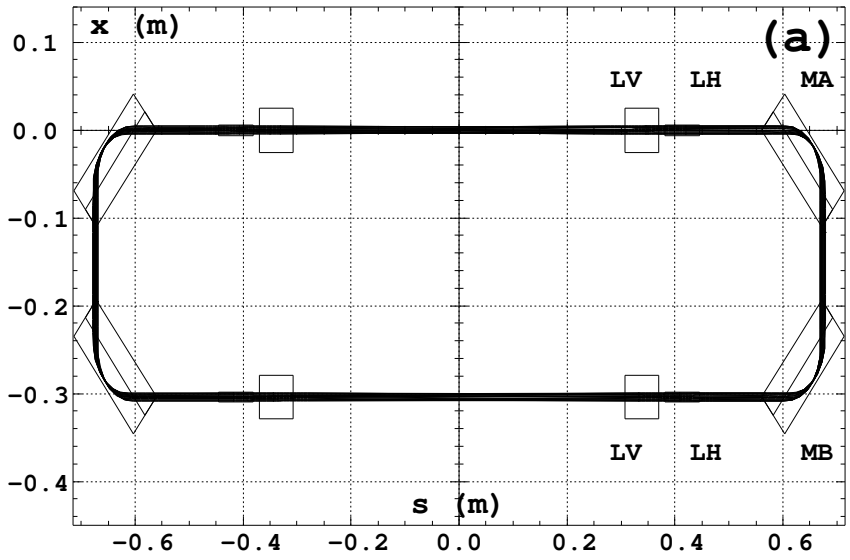

Figure 4: Horizontal beam envelope (from multiturn ray-tracing).

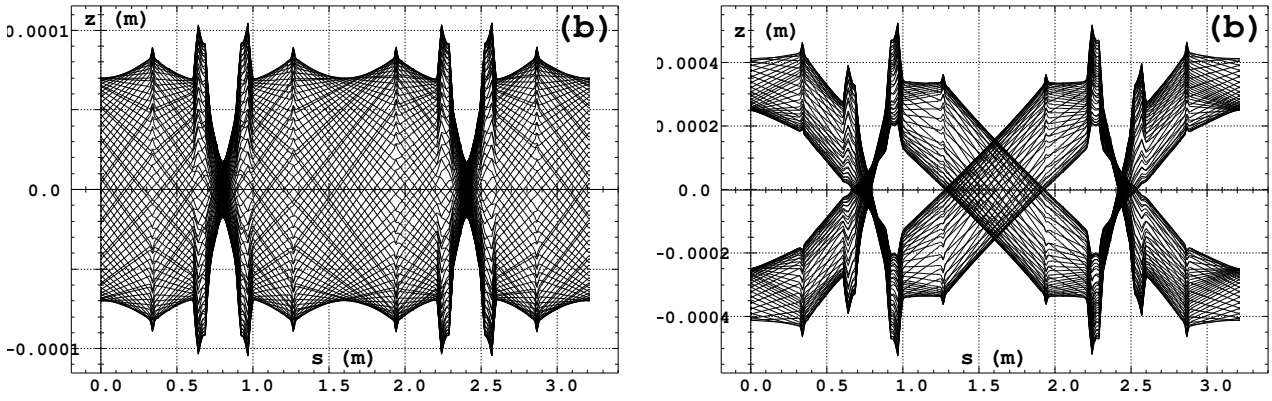

Figure 5: Vertical envelope as generated by multiturn tracking of a particle launched at $s = 0$ with initial coordinates $z'_0 = 0$ and, (a) $z_0 = 0.07\ 10^{-3}$ m (paraxial case), (b) $z_0 = 0.25\ 10^{-3}$ m (large amplitude case with vertical tune $\nu_z \approx$ half integer).

Those features of a noticeably restrained domain of linear behavior determined our resorting to numerical ray-tracing means for further precise investigations regarding large acceptance issues.

4 Geometrical transverse acceptance

The acceptance is evaluated in terms of survival number of turns. For that purpose particles are launched at azimuth $s = 0$ with sampled x_0, z_0 values and tracked up to 1000 turns around the ring ; this may seem quite a large number compared to the few tens of turns necessary for TOFMS operation, however such strong constraint is expected to warrant beam qualities, and in addition it provides a benchmark towards the use of the multiturn device as a long term electrostatic storage ring for possible other applications.

Survival results are summarized in Figs. 6, 7, amenable to the following comments.
The horizontal paraxial tune is set slightly above 1/3 integer using $V_{LH} = 38$ Volts ; this entails very good horizontal geometrical acceptance (Fig. 6) leading in particular to a fair beam occupation of about two thirds the mechanical aperture in the LH lenses. One beneficial effect is in the positive amplitude detuning $d\nu_x/dx_0$ that takes ν_x away from the resonance for increasing amplitudes, up to $\nu_x \approx 0.449$ for the limit excursion $x_0 \approx \pm 4\ 10^{-3}$ m.
The 1000-turn vertical acceptance has been assessed through three tuning cases, $V_{LV} = 60$ Volts ($\nu_z = 2.33$), $V_{LV} = 76$ Volts ($\nu_z = 2.53$) and $V_{LV} = 86$ Volts ($\nu_z = 2.656$) (Fig. 7). The amplitude detuning $d\nu_z/dz_0$ is negative entailing that the vertical acceptance comprises the quarter-integer resonance region in the $V_{LV} = 60$ Volts case and the half-integer one in the $V_{LV} = 76$ Volts case. More linear motion is obtained with $V_{LV} = 86$ Volts and leads to about $\Delta z_0 = \pm 0.8\ 10^{-3}$ m acceptance.

For reference, the corresponding accepted emittances (the surface encompassed by the extreme trajectories in Figs. 6, 7) are

$$A_x/\pi \approx 20\ 10^{-6}\text{m.rad}, \quad A_z/\pi \approx 1.4\ 10^{-6}\text{m.rad} \tag{7}$$

5 6-D acceptance

Acceptance in presence of horizontal and vertical motions and of energy spread is now assessed, by launching a 1000-particle beam with realistic 6-D initial conditions $(x_0, x_0', z_0, z_0', t_0, \delta E/E)$ for multiturn tracking. Horizontal and vertical starting coordinates are sorted at random within Gaussian concentration ellipses whose surface compares with the multiturn acceptance already evaluated (Eq. 7), namely with sigma-values

$$\sigma_x = 4\ 10^{-3}\ \text{m},\ \ \sigma_{x'} = 3.5\ 10^{-3}\ \text{rad},\ \ \sigma_z = 0.4\ 10^{-3}\ \text{m},\ \ \sigma_{z'} = 0.75\ 10^{-3}\ \text{rad} \tag{8}$$

corresponding to approximate injected emittances (in terms of the linear approximation Eq. 3) $\epsilon_x/\pi = 14\ 10^{-6}$ m.rad and $\epsilon_z/\pi = 0.3\ 10^{-6}$ m.rad. The energy is sorted at random within Gaussian distribution with rms value $\sigma_{\delta E/E} \approx 10^{-3}$.

Fig. 8 shows typical results obtained in the $V_{LV} = 76$ Volts case : the total transmission after 100 turns in the ring is 725 particles over 1000 launched; final histograms after 100 turns do not differ much from the starting ones, the main observation being diffusion in the vertical motion, which is not surprising considering the large vertical non-linearities introduced by the electrostatic deflectors.

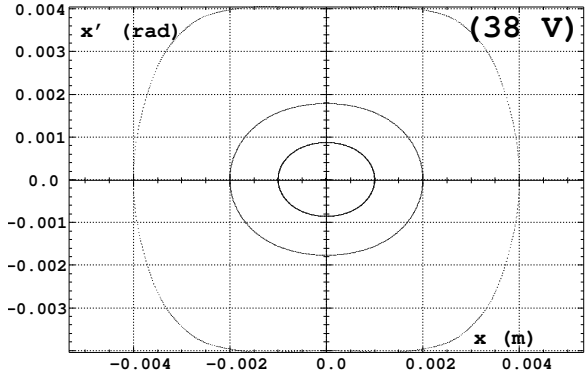

Figure 6: 1000-turn horizontal acceptance as observed at $s = 0$, with $V_{LH} = 38$ Volts, $V_{LV} = 76$ Volts. All particles launched within $|x_0| \leq 8\ 10^{-3}$ m and $\epsilon_z \approx 0$ survive 1000 turns.

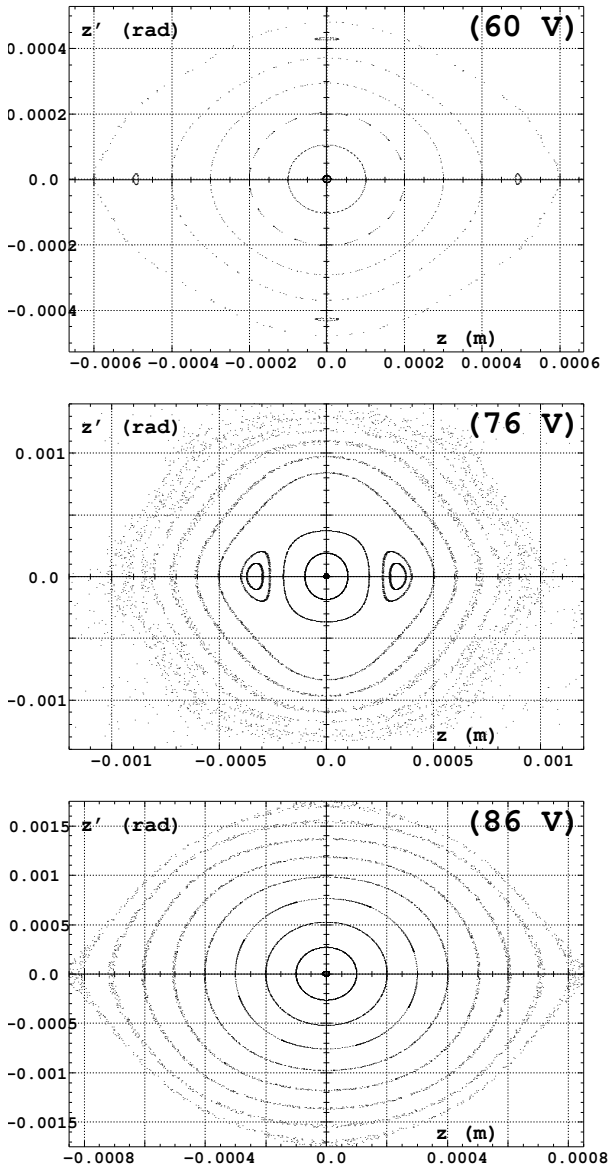

Figure 7: 1000-turn vertical acceptance as observed at $s = 0$, for $V_{LV} = 60, 76$and86 Volts.

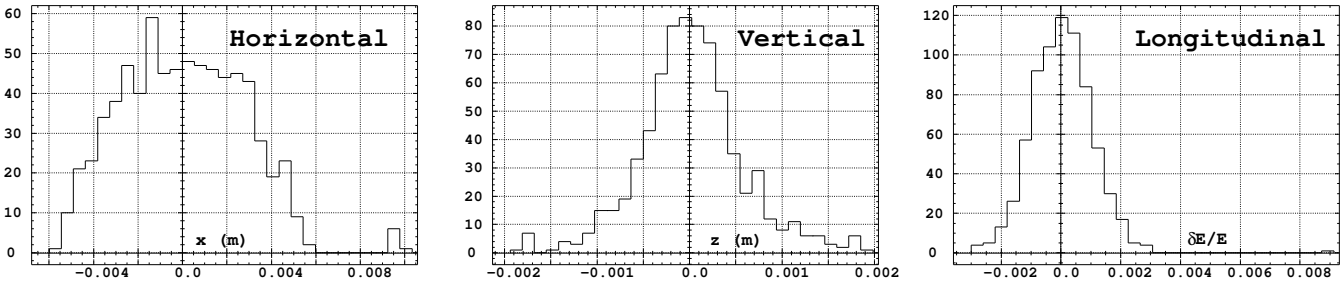

Figure 8: Histograms at $s = 0$ of final $x, z, \delta E/E$ coordinates of the 725/1000 particles that have survived a 100-turn run in the ring, for $V_{LV} = 76$ Volts.

6 Time separation

Time separation is assessed with $V_{LH} = 38$ V and $V_{LV} = 60$ V for illustration. Considered masses differ by 10^{-4}, namely M1=26.082 GeV and M2= $1.0001\times$M1. Two 1000-particle bunches are launched from $s = 0$, assuming identical start time for all particles (i.e., zero bunch length) ; one bunch is filled with M1 exclusively, the other one is filled with M2 ; both have identical mean energy $< E >= 400$ eV.

Starting particle coordinates (x_0, x'_0), (z_0, z'_0) are sorted at random in Gaussian concentration ellipses with emittances $\epsilon_x/\pi = 0.02\ 10^{-6}$ m.rad and $\epsilon_z/\pi = 0.01\ 10^{-6}$ m.rad, well within multiturn acceptance as studied in Section 5 (Eq. 7), probably even too small : indeed, time resolution will be altered by transverse non linearities, which certainly deserves further investigation with more realistic larger emittances. The energy spread $\sigma_{\delta E/E}$ within the bunch is chosen either zero, or non zero as specified further ahead, and in this case sorted at random in a centered Gaussian distribution.

The aim of the game is to determine how many turns are necessary to get the two bunches separated in time. Histograms computed from ray-tracing data, in presence of zero energy spread are shown in Fig. 9 ; the separation comes out to be $0.0126\ 10^{-6}$s/turn, proportional to the number of turns, large enough for efficient time of flight resolution after just a few revolutions, wouldn't it be for the induced longitudinal bunch spread : indeed, tracking data in presence of non-zero $\sigma_{\delta E/E}$ show that bunch lengthening precludes resolution beyond $\delta E/E \approx 10^{-4}$ (Fig. 9).

7 Conclusion

The present study provides guidelines for high accuracy multiturn ray-tracing based investigations regarding a compact electrostatic multiturn time of flight mass spectrometer built from parallel-plate mirrors operated as both deflectors and focusing lenses. Outstanding results can be summarized as follows :

It has been observed that a lattice cell with horizontal acceptance close to the geometrical aperture of the lenses can easily be designed. The vertical acceptance is on its side smaller and very sensitive to the potential applied on the vertical focusing lens, and as well to potentials in the MA and MB deflectors which suggests that possible improvements call for a minimization of the vertical beam envelope in MA, MB. Attention should be given to the compensation of chromatic effects on

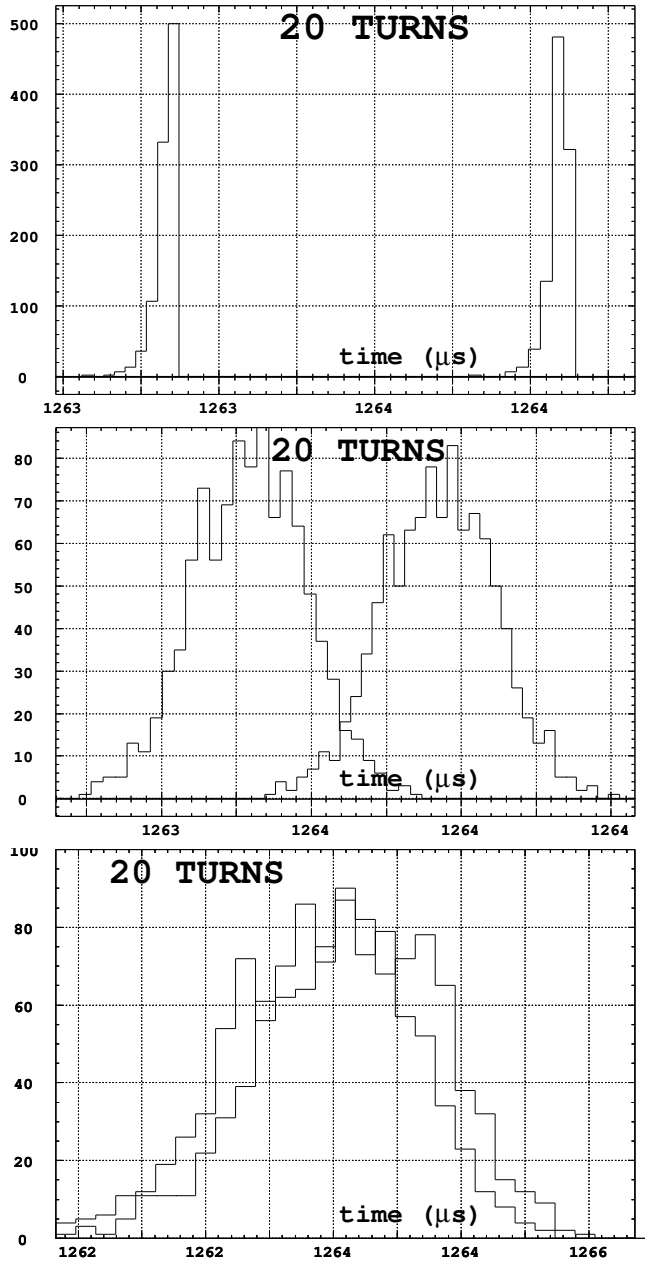

Figure 9: Time of flight histograms of M1 and M2 bunches as observed at s=0 after 20 turns in the TOFMS ring, for energy spread $\delta E/E = 0,\ 10^{-4}$ and 10^{-3}. In all histograms M1 is the left distribution, M2 is the right one.

the one hand so as to increase the 6-D acceptance, on the other hand for improving time separation in presence of per-mil to per-cent scale energy spread by compensation of the bunch lengthening coefficient.

Eventually it can be concluded that, provided such improvements are within reach this type of device is a good candidate for further use as a low energy storage ring.

Appendix

A Numerical integration method

The ray-tracing code Zgoubi used for the present study, solves the Lorentz equation

$$\frac{d(m\vec{v})}{dt} = q\,(\vec{E} + \vec{v} \times \vec{B}) \tag{9}$$

($m, q, \vec{v}$ are respectively the relativistic mass, charge and velocity, $\vec{E}$ and $\vec{B}$ are the electrostatic and magnetostatic fields experienced in the optical elements) by calculating the Taylor expansions

$$\vec{R}(M_1) \approx \vec{R}(M_0) + \vec{u}(M_0)\,\Delta s + \vec{u}^{'}(M_0)\,\frac{\Delta s^2}{2!} + ... + \vec{u}^{''''}(M_0)\,\frac{\Delta s^6}{6!} \tag{10}$$

and

$$(B\rho)(M_1) = (B\rho)(M_0) + (B\rho)^{'}(M_0)\Delta s + ... + (B\rho)^{''''}(M_0)\frac{\Delta s^4}{4!} \tag{11}$$

wherein $\vec{u} = \vec{v}/v$, $ds = v\,dt$, $()' = d()/ds$. $\vec{R}$ is the particle position vector, its value at location M_1 one step Δs ahead is obtained from truncated Taylor expansion at previous location M_0. $B\rho = p/q$ is the rigidity of the particle with momentum $p = mv$. The need for explicit field derivatives appears from the normalized form

$$(B\rho)'\vec{u} + B\rho\,\vec{u}' = \frac{\vec{e}}{v} + \vec{u} \times \vec{b} \tag{12}$$

of Eq. 9 ($\vec{e} = \vec{E}/B\rho$, $\vec{b} = \vec{B}/B\rho$). Note that, things simplify in the present problem of purely electrostatic motion in that all magnetic field terms above vanish.

Calculation of the time of flight

Time of flight in electrostatic fields has been installed in Zgoubi on purpose for the present study ; it follows from similar Taylor series, namely

$$T(M_1) \approx T(M_0) + \frac{dT}{ds}(M_0)\,\Delta s + \frac{d^2T}{ds^2}(M_0)\,\frac{\Delta s^2}{2} + \frac{d^3T}{ds^3}(M_0)\,\frac{\Delta s^3}{3!} + \frac{d^4T}{ds^4}(M_0)\,\frac{\Delta s^4}{4!} \tag{13}$$

The derivatives d^nT/ds^n are obtained from $dT/ds = 1/v$, $d^2T/ds^2 = d(1/v)/ds$, etc. with, after Eq. 12 and in the particular case of zero magnetic field [6]

$$\left(\frac{1}{v}\right)' = \frac{1}{c^2}\,\frac{(\vec{e}\cdot\vec{u})}{B\rho} - \frac{1}{v}\,\frac{(B\rho)'}{B\rho}$$

$$\begin{aligned}\left(\frac{1}{v}\right)'' &= \frac{1}{c^2}\frac{(\vec{e}\cdot\vec{u})'}{B\rho} - 2\left(\frac{1}{v}\right)'\frac{(B\rho)'}{B\rho} - \frac{1}{v}\frac{(B\rho)''}{B\rho} \\ \left(\frac{1}{v}\right)''' &= \frac{1}{c^2}\frac{(\vec{e}\cdot\vec{u})''}{B\rho} - 3\left(\frac{1}{v}\right)''\frac{(B\rho)'}{B\rho} - 3\left(\frac{1}{v}\right)'\frac{(B\rho)''}{B\rho} - \frac{1}{v}\frac{(B\rho)'''}{B\rho}\end{aligned} \tag{14}$$

B The electrostatic parallel-plate mirror/lens

A 3-electrode parallel-plate mirror/lens is schemed in Fig. 10. It is made up of three pairs of parallel

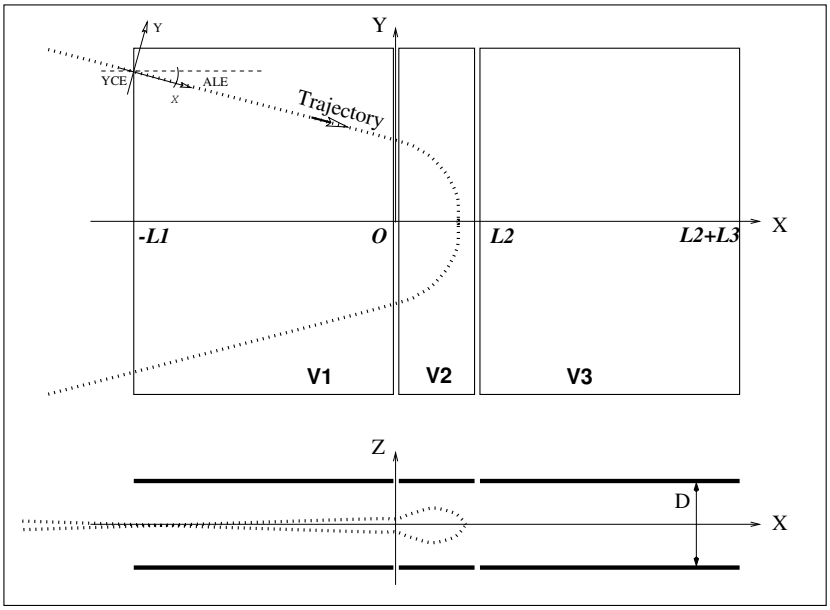

Figure 10: An illustration of the electrostatic 3-electrode mirror/lens with straight slits, used as an horizontal mirror. The dashed curves represent a trajectory.

electrodes and has mid-plane symmetry. Electrode lengths are $L1$, $L2$, $L3$. D is the gap. The model for the electrostatic potential is (after Ref. [3, p.412])

$$V(X,Z) = \sum_{i=2}^{3} \frac{V_i - V_{i-1}}{\pi} \arctan\frac{\sinh(\pi(X - Xi{-}1)/D)}{\cos(\pi Z/D)}$$

wherein Vi are the potentials at the 3 electrode pairs (normally $V1 = 0$ refers to the incident beam energy), Xi are the locations of the slits, X is the distance from the origin taken at the first slit (located at $X1 \equiv 0$ between the first and second electrodes). Note that the model assumes infinite-width electrodes and is therefore Y-independent. The model also assumes zero-width slits, which is valid from a practicle view point as long as the slit width is much smaller than the gap D.

From $V(X,Z)$ the field $\vec{E}(X,Y,Z)$ and its derivatives at current location $M_0(X,Y,Z)$ of the ray-traced particle, as needed in Eqs. 10, 11, 14, are obtained by differentiation (in particular $E_Y(X,Y,Z) = -\partial V(X,Z)/partialY$ and derivatives are identically zero).

The mirror as well as lenses inter-plate gap in the TOFMS (Fig. 1) is $D = 12\ 10^{-3}$ m. The ratio `gap/L2` is of paramount effect and determines in a very sensible way the functioning regime of the lens and mirror (e.g., stigmatic imaging, parallel to parallel imaging, etc.) [8].

References

[1] See for instance,
C. Berger and M. Baril, Les miroirs bicylindriques et leur utilisation dans les spectromètres de masse magnétiques à multiples passages, Rev. Phys. Appl. Tome 13, mai 1978 (271-281).
T. Sakurai, M. Baril, Ion optics of a high resolution multi-passage mass spectrometer with electrostatic mirrors, NIM A 363 (1995) 473-476.
M. Baril, An achromatic multi-passage mass spectrometer, NIM A 427 (1999) 136-140
T. Sakurai, H. Nakabushi, T. Hiasa, K. Okanishi, A new multi-passage TOFMS at JAIST, NIM A 427 (1999) 182-186.

[2] See for instance,
S. Bimurzaev, V. M. Kel'man, E. M. Yakushev, Telescope electrostatic system with removable spherical aberration, Zh. Tekh. Fiz. 46, 452-459 (March 1976), and earlier publications referred to therein by the authors.

[3] S. P. Karetskaya, L. G. Glickman, L. G. Beizina, Yu. V. Goloskokov, Mirror-bank energy analyzers, Advances in electronics and electron optics, vol. 89, Acad. Press. Inc. (1994).

[4] M. Baril, D. Michaud, F. Méot, Design of a purely electrostatic storage ring using the new programming language "*J*" and comparison with other ion optics software, Proc. ICAP2000 Conf., September 11 - 14, 2000, Darmstadt University of Technology (http://www.ICAP2000.de).

[5] M. Baril, F. Méot, D. Michaud, Design study of a compact multiturn time of flight mass spectrometer, report CEA/DSM/DAPNIA/SEA-00-08 *and* Université Laval à Québec UL2000-PHY-B0501, CEA Saclay (2000).

[6] F. Méot and S. Valero, Zgoubi users' guide, report CEA/DSM/DAPNIA/SEA-97-13, CEA Saclay (1997) ; see also, F. Méot, the ray-tracing code Zgoubi, NIM A 427 (1999) 353-356.

[7] David A. Dahl, SIMION 3D Version 6.0, 43rd ASMS Conference on Mass Spectrometry and Allied Topics, May 21-26 1995, Atlanta, Georgia, pg 717 ; http://www.sisweb.com/simion.htm.

[8] S. Bimurzaev, Report on business trip to Laval University (unpublished), Kazakh State Nat. University, Physics Department, July 27 - August 26, 1998.

[9] U.S. patent # 6,037,586, March 2000.

[10] K. L. Brown and R. V. Servanckx, Fisrt- and second-order charged particle optics, AIP Conf. Proc. 127 pp.64-138 , M. Month ed., New York 1985.